

A MIXED FINITE ELEMENT METHOD FOR NEARLY INCOMPRESSIBLE MULTIPLE-NETWORK POROELASTICITY *

J. J. LEE[†], E. PIERSANTI[‡], K.-A. MARDAL[§], AND M. E. ROGNES[¶]

Abstract. In this paper, we present and analyze a new mixed finite element formulation of a general family of quasi-static multiple-network poroelasticity (MPET) equations. The MPET equations describe flow and deformation in an elastic porous medium that is permeated by multiple fluid networks of differing characteristics. As such, the MPET equations represent a generalization of Biot's equations, and numerical discretizations of the MPET equations face similar challenges. Here, we focus on the nearly incompressible case for which standard mixed finite element discretizations of the MPET equations perform poorly. Instead, we propose a new mixed finite element formulation based on introducing an additional total pressure variable. By presenting energy estimates for the continuous solutions and *a priori* error estimates for a family of compatible semi-discretizations, we show that this formulation is robust in the limits of incompressibility, vanishing storage coefficients, and vanishing transfer between networks. These theoretical results are corroborated by numerical experiments. Our primary interest in the MPET equations stems from the use of these equations in modelling interactions between biological fluids and tissues in physiological settings. So, we additionally present physiologically realistic numerical results for blood and tissue fluid flow interactions in the human brain.

Key words. multiple-network poroelasticity, mixed finite element, incompressible, cerebral fluid flow

AMS subject classifications. 65M12, 65M15, 65M60, 92C10

1. Introduction. In this paper, we consider a family of quasi-static multiple-network poroelasticity (MPET¹) equations reading as follows: for a given number of networks $A \in \mathbb{N}$, find the displacement u and the network pressures p_j for $j = 1, \dots, A$ such that

$$(1.1a) \quad -\operatorname{div} C\varepsilon(u) + \sum_j \alpha_j \nabla p_j = f,$$

$$(1.1b) \quad c_j \dot{p}_j + \alpha_j \operatorname{div} \dot{u} - \operatorname{div} K_j \nabla p_j + S_j = g_j, \quad 1 \leq j \leq A,$$

where $u = u(x, t)$ and $p_j = p_j(x, t)$, $1 \leq j \leq A$ for $x \in \Omega \subset \mathbb{R}^d$ ($d = 1, 2, 3$) and for $t \in [0, T]$.

In our context, (1.1) originates from balance of mass and momentum in a porous, linearly elastic medium permeated by A segregated viscous fluid networks. The operators and parameters are as follows: C is the elastic stiffness tensor, each network

*Submitted to the editors April 23, 2018.

Funding: The work of J. J. Lee has been supported by the European Research Council under the European Union's Seventh Framework Programme (FP7/2007-2013) ERC grant agreement 339643. The work of M. E. Rognes and K.-A. Mardal have been supported by the Research Council of Norway under the FRINATEK Young Research Talents Programme through project #250731/F20 (Waterscape). E. Piersanti is a doctoral fellow in the Simula-UCSD-University of Oslo Research and PhD training (SUURPh) program, an international collaboration in computational biology and medicine funded by the Norwegian Ministry of Education and Research.

[†]Institute for Computational Engineering and Sciences, The University of Texas at Austin, 201 E. 24th Street, POB 4.102, Austin, Texas 78712, USA (johnlee04@gmail.com)

[‡]Simula Research Laboratory, P. O. Box 134, 1325 Lysaker, Norway (eleonora@simula.no)

[§]Department of Mathematics, University of Oslo, P. O. Box 1053 Blindern, 0316 Oslo, Norway and Simula Research Laboratory, P. O. Box 134, 1325 Lysaker, Norway (kent-and@simula.no)

[¶]Simula Research Laboratory, P. O. Box 134, 1325 Lysaker, Norway (meg@simula.no)

¹The abbreviation MPET stems from the term multiple-network poroelastic theory as used by e.g. [35]. Here, we instead refer to the multiple-network poroelasticity equations but keep the abbreviation for the sake of convenience.

j is associated with a Biot-Willis coefficient $\alpha_j \in (0, 1]$, storage coefficient $c_j \geq 0$, and hydraulic conductivity tensor $K_j = \kappa_j / \mu_j > 0$ (where κ_j and μ_j represent the network permeability and the network fluid viscosity, respectively). In (1.1a), ∇ denotes the gradient, ε is the symmetric (row-wise) gradient, div denotes the row-wise divergence. In (1.1b), ∇ and div are the standard gradient and divergence operators, and the superposed dot denotes the time derivative. Further, f represents a body force and g_j represents sources in network j for $j = 1, \dots, A$, while S_j represents transfer terms out of network j .

In this paper, we consider the case of an isotropic stiffness tensor for which

$$(1.2) \quad C\varepsilon(u) = 2\mu\varepsilon(u) + \lambda \text{div } uI$$

where μ, λ are the standard non-negative Lamé parameters and I denotes the identity tensor. Moreover, we will consider the case where the transfer terms S_j , quantifying the transfer out of network j into the other fluid networks, are proportional to pressure differences between the networks. More precisely, we assume that S_j takes the form:

$$(1.3) \quad S_j = S_j(p_1, \dots, p_A) = \sum_{i=1}^A \xi_{j \leftarrow i} (p_j - p_i),$$

where $\xi_{j \leftarrow i}$ are non-negative transfer coefficients for $i, j = 1, \dots, A$. We will also assume that these transfer coefficients are symmetric in the sense that $\xi_{j \leftarrow i} = \xi_{i \leftarrow j}$, and note that $\xi_{j \leftarrow j}$ is arbitrary.

The MPET equations have an abundance of both geophysical and biological applications. In the case $A = 1$, (1.1) reduces to the well-known quasi-static Biot equations. While the Biot equations have been studied extensively, see e.g. [32, 25, 29, 2, 28, 22, 38]; to the best of our knowledge, the general multiple-network poroelasticity equations have received much less attention, especially from the numerical perspective. The case $A = 2$ is known as the Barenblatt-Biot model, and we note that Showalter and Momken [33] present an existence analysis for this model, while Nordbotten and co-authors [27] present an *a posteriori* error analysis for an approximation of a static Barenblatt-Biot system.

Our interest in the multiple-network poroelasticity equations primarily stems from the use of these equations in modelling interactions between biological fluids and tissue in physiological settings. As one example, Tully and Ventikos [35] considers (1.1) with four different networks ($A = 4$) to model fluid flows, network pressures and elastic displacement in brain tissue. The fluid networks represent the arteries, the arterioles/capillaries, the veins and the interstitial fluid-filled extracellular space, each network with e.g. a different permeability κ_j and different transfer coefficients $\xi_{j \leftarrow i}$.

A particularly important motivation for the current work is the recently proposed theory of the glymphatic system which describes a new mechanism for waste clearance in the human brain [18, 19, 1]. This mechanism is proposed to take the form of a convective flow of water-like fluid through (a) spaces surrounding the cerebral vasculature (paravascular spaces) and (b) through the extracellular spaces, driven by a hydrostatic pressure gradient between the arterial and venous compartments. Compared to diffusion only, such a convective flow would lead to enhanced transport of solutes through the brain parenchyma and, in particular, contribute to clearance of metabolic waste products such as amyloid beta. The accumulation of amyloid beta frequently seen in patients with Alzheimer's disease is as such seen as a malfunction of the glymphatic system. In this context, the original system of [35] represents a macroscopic model of interaction between the different fluid networks in the brain.

Discretization of Biot's equations is known to be challenging, in particular because of so-called poroelastic locking. Poroelastic locking has two main characteristics: 1) underestimation of the solid deformation if the material is close to being incompressible and 2) nonphysical pressure oscillations, in particular in the areas close to jumps in the permeabilities or to the boundary. Several recent (and not so recent) studies, see e.g. [29, 6, 4, 17, 31, 38], focus on a three-field formulation of Biot's model, involving the elastic displacement, fluid pressure and fluid velocity. Four-field formulations where also the elasticity equation is in mixed form, designed to provide robust numerical methods for nearly incompressible materials, have also been studied [37, 20, 21].

In biological tissues, any jumps in the permeability parameters are typically small in contrast to geophysical applications. The challenge in the biomedical applications is rather that the tissues in our body mostly consist of water and as such should be close to be incompressible (for short time-scales and normal physiological pressures). Therefore, it may be crucial for accurate modeling of the interaction of the different network pressures in (1.1) to allow for an elastic material that is almost incompressible and/or with (nearly) vanishing storage coefficients, i.e. for $1 \ll \lambda < +\infty$ and $0 < c_j \ll 1$ in (1.1). Standard two-field mixed finite element discretizations of the Biot model, approximating the displacement and the fluid pressure only using Stokes-stable elements, are well-known to perform poorly in the incompressible limit, see e.g. [22] and references therein. Moreover, we can easily demonstrate a suboptimal convergence rate for the corresponding standard mixed finite element discretization of the MPET equations, see Example 1.1 below. On the other hand, two-field approximations are computationally inexpensive compared to three-field approximations in the sense that only one unknown, the network pressure, is involved in each network.

EXAMPLE 1.1. *To illustrate poor performance of a standard mixed finite element discretization of the MPET equations (1.1) in the nearly incompressible case, we consider a variant of the smooth test case presented by [38, Section 7.1]. Let $\Omega = [0, 1]^2 \subset \mathbb{R}^2$, take $T = 0.5$, and consider the quasi-static multiple-network poroelasticity equations (1.1) with $A = 2$, $c_j = 1.0$, $K_j = 1.0$, $\alpha_j = 1.0$, and $S_j = 0$ for $j = 1, 2$. Moreover, we let $E = 1.0$ and $\nu = 0.49999$ for*

$$\mu = \frac{E}{2(1+\nu)} \approx \frac{1}{3}, \quad \lambda = \frac{\nu E}{(1-2\nu)(1+\nu)} \approx 16\,666.$$

To discretize (1.1), we consider a Crank-Nicolson discretization in time and a standard mixed finite element discretization in space in this example. More precisely, we approximate the displacement u using continuous piecewise quadratic vector fields (and denote the approximation by u_h) and the fluid pressures p_j for $j = 1, 2$ using continuous piecewise linears defined relative to a uniform mesh of Ω of mesh size h . As exact solutions, we let

$$u((x_0, x_1), t) = t \begin{pmatrix} (\sin(2\pi x_1)(-1 + \cos(2\pi x_0)) + \frac{1}{\mu+\lambda} \sin(\pi x_0) \sin(\pi x_1)) \\ (\sin(2\pi x_0)(1 - \cos(2\pi x_1)) + \frac{1}{\mu+\lambda} \sin(\pi x_0) \sin(\pi x_1)) \end{pmatrix},$$

and

$$p_j((x_0, x_1), t) = -jt \sin(\pi x_0) \sin(\pi x_1).$$

The resulting approximation errors for $u(T)$ in the $L^2(\Omega)$ and $H^1(\Omega)$ norms are listed in Table 1 for a series of meshes generated by nested uniform refinements, together

with the corresponding rates of convergence. We observe that the convergence rates are one order sub-optimal for this choice of spatial discretization.

h	$\ u(T) - u_h(T)\ $	Rate	$\ u(T) - u_h(T)\ _{H^1}$	Rate
H	0.169		2.066	
$H/2$	0.040	2.09	0.980	1.08
$H/4$	0.010	2.04	0.480	1.03
$H/8$	0.002	2.03	0.235	1.03
$H/16$	0.001	2.09	0.110	1.10
Optimal		3		2

Table 1: Approximation errors in the L^2 ($\|\cdot\|$)- and H^1 ($\|\cdot\|_{H^1}$)-norms and associated convergence rates for a standard mixed finite element discretization for a smooth manufactured solution test case for a nearly incompressible material (Example 1.1). H corresponds to a uniform mesh constructed by dividing the unit square into 4×4 squares and dividing each square by a diagonal.

The primary objective of this paper is to propose and analyze a new variational formulation and a corresponding spatial discretization of the MPET equations that are robust with respect to a nearly incompressible poroelastic matrix; i.e. the implicit constants in the error estimates are uniformly bounded for arbitrarily large $\lambda > 0$. To this end, we introduce a formulation with one additional scalar field unknown. For the MPET equations (1.1) with potentially multiple networks, the additional computational cost is thus small. Instead of taking the "solid pressure" $\lambda \operatorname{div} u$ as a new unknown, we take the total pressure, which is defined as a weighted sum of the network pressures and the solid pressure, as the new unknown. Such a formulation has previously been shown to be advantageous in the context of parameter-robust preconditioners for the Biot model [23]. Here, we focus on stability and error estimates of the total pressure formulation for the more general MPET equations. The construction of preconditioners for the MPET equations will be addressed in a forthcoming paper.

Our new theoretical results include an energy estimate for the continuous variational formulation that is robust in the relevant parameter limits, in particular, that is uniform in the Lamé parameter λ , storage coefficients c_j for $j = 1, \dots, A$, and transfer coefficients $\xi_{j \leftarrow i}$ for $i, j = 1, \dots, A$, and a robust *a priori* error estimate for a class of compatible semi-discretizations of the new formulation. These theoretical results are supported by numerical experiments. Finally, we also present new numerical MPET simulations modelling blood and tissue fluid interactions in a physiologically realistic human brain.

This paper is organized as follows. Section 2 presents notation and general preliminaries. In Section 3, we introduce a total-pressure-based variational formulation (3.6) for the quasi-static MPET equations (1.1), together with a robust energy estimate in Theorem 3.3. We continue in Section 4 by proposing a general class of compatible semi-discretizations (4.1) of this formulation, and estimate the *a priori* discretization errors in Proposition 4.1 and the semi-discrete errors for a specific choice of finite element spaces in Theorem 4.2 and Proposition 4.4. These theoretical results are corroborated by synthetic numerical convergence experiments in Section 5. In Section 6,

we present a more physiologically realistic numerical experiment using a 4-network MPET model to investigate blood and tissue fluid flow in the human brain. Some conclusions and directions of future research are highlighted in Section 7.

2. Notation and preliminaries. Throughout this paper we use $X \lesssim Y$ to denote the inequality $X \leq CY$ with a generic constant $C > 0$ which is independent of mesh sizes. If needed, we will write C explicitly in inequalities but it can vary across expressions.

2.1. Sobolev spaces. Let Ω be a bounded polyhedral domain in \mathbb{R}^d ($d = 1, 2$, or 3) with boundary $\partial\Omega$. We let $L^2(\Omega)$ be the set of square-integrable real-valued functions on Ω . The inner product of $L^2(\Omega)$ and the induced norm are denoted by $\langle \cdot, \cdot \rangle$ and $\| \cdot \|$, respectively. For a finite-dimensional inner product space \mathbb{X} , typically $\mathbb{X} = \mathbb{R}^d$, let $L^2(\Omega; \mathbb{X})$ be the space of \mathbb{X} -valued functions such that each component is in $L^2(\Omega)$. The inner product of $L^2(\Omega; \mathbb{X})$ is naturally defined by the inner product of \mathbb{X} and $L^2(\Omega)$, so we use the same notation $\langle \cdot, \cdot \rangle$ and $\| \cdot \|$ to denote the inner product and norm on $L^2(\Omega; \mathbb{X})$. For a non-negative real-valued function on Ω (or symmetric positive semi-definite tensor-valued function on Ω) w , we also introduce the short-hand notations

$$(2.1) \quad \langle u, v \rangle_w = \langle wu, v \rangle, \quad \|u\|_w^2 = \langle u, u \rangle_w,$$

noting that the latter is a norm only when w is strictly positive a.e. on Ω (or is positive definite a.e. on Ω).

For a non-negative integer m , $H^m(\Omega)$ denotes the standard Sobolev spaces of real-valued functions based on the L^2 -norm, and $H^m(\Omega; \mathbb{X})$ is defined similarly based on $L^2(\Omega; \mathbb{X})$. To avoid confusion with the weighted L^2 -norms cf. (2.1) we use $\| \cdot \|_{H^m}$ to denote the H^m -norm (both for $H^m(\Omega)$ and $H^m(\Omega; \mathbb{X})$). For $m \geq 1$, we use $H_{0,\Gamma}^m(\Omega)$ to denote the subspace of $H^m(\Omega)$ with vanishing trace on $\Gamma \subset \partial\Omega$, and $H_{0,\Gamma}^m(\Omega; \mathbb{X})$ is defined similarly [14]. For $\Gamma = \partial\Omega$, we write $H_0^m(\Omega)$ and analogously $H_0^m(\Omega; \mathbb{X})$.

2.2. Spaces involving time. We will consider an interval $[0, T]$, $T > 0$. For a reflexive Banach space \mathcal{X} , let $C^0([0, T]; \mathcal{X})$ denote the set of functions $f : [0, T] \rightarrow \mathcal{X}$ that are continuous in $t \in [0, T]$. For an integer $m \geq 1$, we define

$$C^m([0, T]; \mathcal{X}) = \{f \mid \partial^i f / \partial t^i \in C^0([0, T]; \mathcal{X}), 0 \leq i \leq m\},$$

where $\partial^i f / \partial t^i$ is the i -th time derivative in the sense of the Fréchet derivative in \mathcal{X} (see e.g. [39]).

For a function $f : [0, T] \rightarrow \mathcal{X}$, we define the space-time norm

$$\|f\|_{L^r([0, T]; \mathcal{X})} = \begin{cases} \left(\int_0^T \|f(s)\|_{\mathcal{X}}^r ds \right)^{1/r}, & 1 \leq r < \infty, \\ \text{ess sup}_{t \in [0, T]} \|f(t)\|_{\mathcal{X}}, & r = \infty. \end{cases}$$

We define the space-time Sobolev spaces $W^{k,r}([0, T]; \mathcal{X})$ for a non-negative integer k and $1 \leq r \leq \infty$ as the closure of $C^k([0, T]; \mathcal{X})$ with the norm $\|f\|_{W^{k,r}([0, T]; \mathcal{X})} = \sum_{i=0}^k \|\partial^i f / \partial t^i\|_{L^r([0, T]; \mathcal{X})}$.

2.3. Finite element spaces. Let \mathcal{T}_h be an admissible, conforming, simplicial tessellation of the domain Ω . For any integer $k \geq 1$, we let $\mathcal{P}_k(\mathcal{T}_h)$ denote the space of continuous piecewise polynomials of order k defined relative to \mathcal{T}_h , and $\mathcal{P}_k^d(\mathcal{T}_h)$ as the space of d -tuples with components in \mathcal{P}_k . We will typically omit the reference to \mathcal{T}_h

when context allows. We let \mathcal{P}_k° denote the restriction of these piecewise polynomial spaces to conform with given essential homogeneous boundary conditions.

2.4. Parameter values. Based on physical considerations and typical applications, we will make the following assumptions on the material parameter values. First, we assume that the Biot-Willis coefficients $\alpha_j \in (0, 1]$, $j = 1, \dots, A$, and the storage coefficients $c_j > 0$ are constant in time for $j = 1, \dots, A$. In the analysis, we will pay particular attention to robustness of estimates with respect to arbitrarily large λ and arbitrarily small (but not vanishing) c_j 's. We also comment on the case $c_j = 0$ in Remark 4.3.

We will assume that the hydraulic conductivities K_j are constant in time, but possibly spatially-varying and that these satisfy standard ellipticity constraints: i.e. there exist positive constants K_j^- and K_j^+ such that

$$K_j^- \leq K_j(x) \leq K_j^+ \quad \forall x \in \Omega.$$

We assume that the transfer coefficients $\xi_{j \leftarrow i}$ are constant in time and non-negative: i.e. $\xi_{j \leftarrow i}(x) \geq 0$ for $1 \leq i, j \leq A$, $x \in \Omega$.

2.5. Boundary conditions. We will consider (1.1) augmented by the following standard boundary conditions. First, we assume that the boundary decomposes in two parts: $\partial\Omega = \Gamma_D \cup \Gamma_N$ with $\Gamma_D \cap \Gamma_N = \emptyset$ and $|\Gamma_D|, |\Gamma_N| > 0$ where $|\Gamma|$ is the Lebesgue measure of Γ . We use n to denote the outward unit normal vector field on $\partial\Omega$. Relative to this partition, we consider the homogeneous boundary conditions

$$(2.2a) \quad u = 0 \quad \text{on } \Gamma_D,$$

$$(2.2b) \quad C\varepsilon(u) \cdot n = 0 \quad \text{on } \Gamma_N,$$

$$(2.2c) \quad p_j = 0 \quad \text{on } \partial\Omega \quad \text{for } j = 1, \dots, A.$$

The subsequent formulation and analysis can easily be extended to cover inhomogeneous and other types of boundary conditions.

2.6. Key inequalities. For the space $V = H_{0,\Gamma_D}^1(\Omega)$, Korn's inequality [9, p. 288] holds; i.e. there exists a constant $C > 0$ depending only on Ω and Γ_D such that

$$(2.3) \quad \|u\| \leq C\|\varepsilon(u)\| \quad \forall u \in V.$$

Furthermore, for the combination of spaces V and $Q_0 = L^2(\Omega)$, the following (continuous Stokes) inf-sup condition holds: there exists a constant $C > 0$ depending only on Ω and Γ_D such that

$$(2.4) \quad \sup_{u \in V} \frac{\langle \operatorname{div} u, q \rangle}{\|u\|_{H^1}} \geq C\|q\| \quad \forall q \in L^2(\Omega).$$

Our discretization schemes will also satisfy corresponding discrete versions of Korn's inequality and the inf-sup condition with constants independent of the discretization.

2.7. Initial conditions. The MPET equations (1.1) must also be complemented by appropriate initial conditions. In particular, in agreement with the assumption that $c_j > 0$ for $j = 1, \dots, A$, we assume that initial conditions are given for all p_j :

$$(2.5) \quad p_j(x, 0) = p_j^0(x), \quad x \in \Omega, \quad j = 1, \dots, A.$$

Given such p_j^0 , we note that we may compute $u(x, 0) = u^0(x)$ from (1.1a), which in particular yields a $\operatorname{div} u(x, 0) = \operatorname{div} u^0(x)$ for $x \in \Omega$. In the following, we will assume that any initial conditions given are compatible in the sense described here.

3. A new formulation for multiple-network poroelasticity. In this section, we introduce a new variational formulation for the quasi-static multiple-network poroelasticity equations targeting the incompressible and nearly incompressible regime. Inspired by [28, 23], we introduce an additional variable, namely the *total pressure*. In the subsequent subsections, we present the augmented governing equations, introduce a corresponding variational formulation, and demonstrate the robustness of this formulation via an energy estimate.

3.1. Governing equations introducing the total pressure. Let u and p_j for $j = 1, \dots, A$ be solutions of (1.1) with boundary conditions given by (2.2), initial conditions given by (2.5) and recall the isotropic stiffness tensor assumption, cf. (1.2). Additionally, we now introduce the total pressure p_0 defined as

$$(3.1) \quad p_0 = \lambda \operatorname{div} u - \sum_{j=1}^A \alpha_j p_j.$$

Defining $\alpha_0 = 1$ for the purpose of short-hand, and rearranging, we thus have that

$$(3.2) \quad \operatorname{div} u = \lambda^{-1} \sum_{i=0}^A \alpha_i p_i.$$

For simplicity, we denote $\alpha = (\alpha_0, \alpha_1, \dots, \alpha_A)$ and $p = (p_0, p_1, \dots, p_A)$, and we can thus write

$$\sum_{i=0}^A \alpha_i p_i = \alpha \cdot p$$

in the following.

Inserting (3.2) and its time-derivative into (1.1b), we obtain an augmented system of quasi-static multiple-network poroelasticity equations: for $t \in (0, T]$, find the displacement vector field u and the pressure scalar fields p_i for $i = 0, \dots, A$ such that

$$(3.3a) \quad \operatorname{div} u - \lambda^{-1} \alpha \cdot p = 0,$$

$$(3.3b) \quad -\operatorname{div}(2\mu\varepsilon(u) + p_0 I) = f,$$

$$(3.3c) \quad c_j \dot{p}_j + \alpha_j \lambda^{-1} \alpha \cdot \dot{p} - \operatorname{div}(K_j \nabla p_j) + S_j = g_j \quad j = 1, \dots, A.$$

We note that $p_0(x, 0)$ can be computed from (2.5) and (3.1).

REMARK 3.1. *In the limit $\lambda = \infty$, the equations for the displacement u and total pressure p_0 , and the network pressures p_i decouple, and (3.3) reduces to a Stokes system for (u, p_0) and a system of parabolic equations for p_j :*

$$\begin{aligned} -\operatorname{div}(2\mu\varepsilon(u) + p_0 I) &= f, \\ \operatorname{div} u &= 0, \\ c_j \dot{p}_j - \operatorname{div}(K_j \nabla p_j) + S_j &= g_j \quad j = 1, \dots, A. \end{aligned}$$

We next present and study a continuous variational formulation based on the total pressure formulation (3.3) of the quasi-static multiple-network poroelasticity equations.

3.2. Variational formulation. With reference to the notation for domains and Sobolev spaces as introduced in Section 2, let

$$(3.5) \quad V = H_{0,\Gamma_D}^1(\Omega; \mathbb{R}^d), \quad Q_0 = L^2(\Omega), \quad Q_j = H_0^1(\Omega) \quad j = 1, \dots, A.$$

Also denote $Q = Q_0 \times Q_1 \times \cdots \times Q_A$.

Multiplying (3.3) by test functions and integrating by parts with boundary conditions given by (2.2) and initial conditions given by (2.5) yield the following variational formulation: given compatible u^0 and p_j^0 , f and g_j for $j = 1, \dots, A$, find $u \in C^1([0, T]; V)$ and $p_i \in C^1([0, T], Q_i)$ for $i = 0, \dots, A$ such that

$$(3.6a) \quad \langle 2\mu\varepsilon(u), \varepsilon(v) \rangle + \langle p_0, \operatorname{div} v \rangle = \langle f, v \rangle \quad \forall v \in V,$$

$$(3.6b) \quad \langle \operatorname{div} u, q_0 \rangle - \langle \lambda^{-1} \alpha \cdot p, q_0 \rangle = 0 \quad \forall q_0 \in Q_0,$$

$$(3.6c) \quad \langle c_j \dot{p}_j + \alpha_j \lambda^{-1} \alpha \cdot \dot{p} + S_j, q_j \rangle + \langle K_j \nabla p_j, \nabla q_j \rangle = \langle g_j, q_j \rangle \quad \forall q_j \in Q_j,$$

for $j = 1, \dots, A$ and such that $u(\cdot, 0) = u^0(\cdot)$ and $p_j(\cdot, 0) = p_j^0(\cdot)$ for $j = 1, \dots, A$.

The following lemma is a modified version of Lemma 3.1 in [21] and will be used in the energy estimates below. For the sake of completeness, we present its proof here.

LEMMA 3.2. *Let \mathcal{F} , \mathcal{G} , \mathcal{G}_1 , $\mathcal{X} : [0, T] \rightarrow \mathbb{R}$ be continuous, non-negative functions. Suppose that $\mathcal{X}(t)$ satisfies*

$$(3.7) \quad \mathcal{X}^2(t) \leq C_0 \mathcal{X}^2(0) + C_1 \mathcal{X}(0) + \mathcal{G}_1(t) + \int_0^t [\mathcal{F}(s) \mathcal{X}(s) + \mathcal{G}(s)] \, ds,$$

for all $t \in [0, T]$ with constants $C_0 \geq 1$ and $C_1 > 0$. Then for any $t \in [0, T]$,

$$(3.8) \quad \mathcal{X}(t) \lesssim \mathcal{X}(0) + \max \left\{ C_1 + \int_0^t \mathcal{F}(s) \, ds, \left(\mathcal{G}_1(t) + \int_0^t \mathcal{G}(s) \, ds \right)^{\frac{1}{2}} \right\}.$$

Proof. It suffices to show the estimate for the smallest t such that

$$\mathcal{X}(t) = \max_{s \in [0, T]} \mathcal{X}(s).$$

By this assumption, $\mathcal{X}(t) = \max_{s \in [0, T]} \mathcal{X}(s)$ and $\mathcal{X}(s) < \mathcal{X}(t)$ for all $0 \leq s < t$. We now consider two cases: either

$$(3.9) \quad C_1 \mathcal{X}(0) + \int_0^t \mathcal{F}(s) \mathcal{X}(s) \, ds \geq \mathcal{G}_1(t) + \int_0^t \mathcal{G}(s) \, ds$$

or

$$(3.10) \quad C_1 \mathcal{X}(0) + \int_0^t \mathcal{F}(s) \mathcal{X}(s) \, ds < \mathcal{G}_1(t) + \int_0^t \mathcal{G}(s) \, ds.$$

If (3.9) holds, then (3.7) gives

$$\begin{aligned} \mathcal{X}^2(t) &\leq C_0 \mathcal{X}^2(0) + 2C_1 \mathcal{X}(0) + 2 \int_0^t \mathcal{F}(s) \mathcal{X}(s) \, ds \\ &\leq C_0 \mathcal{X}^2(0) + 2C_1 \mathcal{X}(0) + 2\mathcal{X}(t) \int_0^t \mathcal{F}(s) \, ds. \end{aligned}$$

Dividing both sides by $\mathcal{X}(t)$ yields (3.8) because $\mathcal{X}(t) \geq \mathcal{X}(0)$.

On the other hand, if (3.10) is the case, then (3.7) gives

$$\mathcal{X}^2(t) \leq C_0 \mathcal{X}^2(0) + 2\mathcal{G}_1(t) + 2 \int_0^t \mathcal{G}(s) \, ds,$$

and taking the square roots of both sides gives (3.8). \square

Theorem 3.3 below establishes a basic energy estimate for solutions of (3.6), but also for solutions with an additional right-hand side (for the sake of reuse in the *a priori* error estimates).

THEOREM 3.3 (Energy estimate for quasi-static multiple-network poroelasticity).

For given $f \in C^1([0, T]; L^2(\Omega))$, $\beta \in C^1([0, T]; L^2(\Omega))^{A+1}$ and $\gamma_j \in L^2([0, T]; L^2(\Omega))$ for $j = 1, \dots, A$, assume that $u \in C^1([0, T]; V)$ and $p_i \in C^1([0, T]; Q_i)$ for $i = 0, \dots, A$ solve

$$(3.11a) \quad \langle 2\mu \varepsilon(u), \varepsilon(v) \rangle + \langle p_0, \operatorname{div} v \rangle = \langle f, v \rangle \quad \forall v \in V,$$

$$(3.11b) \quad \langle \operatorname{div} u, q_0 \rangle - \langle \lambda^{-1} \alpha \cdot p, q_0 \rangle = \langle g_0, q_0 \rangle \quad \forall q_0 \in Q_0,$$

$$(3.11c) \quad \langle c_j \dot{p}_j + \alpha_j \lambda^{-1} \alpha \cdot \dot{p} + S_j, q_j \rangle + \langle K_j \nabla p_j, \nabla q_j \rangle = \langle g_j, q_j \rangle \quad \forall q_j \in Q_j,$$

for $j = 1, \dots, A$ and $u(0) = u^0$ and $p_j(0) = p_j^0$ for $j = 1, \dots, A$, and where $g_0 = -\lambda^{-1} \alpha \cdot \beta$ and $g_j = \gamma_j + \alpha_j \lambda^{-1} \alpha \cdot \dot{\beta}$ for $j = 1, \dots, A$. Then the following energy estimate holds for all $t \in (0, T]$:

$$(3.12) \quad \|\varepsilon(u(t))\|_{2\mu} + \sum_{j=1}^A \|p_j(t)\|_{c_j} + \|\alpha \cdot p(t)\|_{\lambda^{-1}} \\ + \left(\int_0^t \sum_{j=1}^A \|\nabla p_j\|_{K_j}^2 + \sum_{i,j=1}^A \|p_j - p_i\|_{\xi_{j \leftarrow i}}^2 ds \right)^{\frac{1}{2}} \\ \lesssim I_0 + \int_0^t \left[\|\dot{f}\| + \|\alpha \cdot \dot{\beta}\|_{\lambda^{-1}} \right] ds + \left(\|f(t)\|^2 + \int_0^t \sum_{j=1}^A \|\gamma_j\|^2 ds \right)^{\frac{1}{2}},$$

where

$$(3.13) \quad I_0 = \|\varepsilon(u(0))\|_{2\mu} + \sum_{j=1}^A \|p_j(0)\|_{c_j} + \|\alpha \cdot p(0)\|_{\lambda^{-1}} + \|f(0)\|,$$

and where the inequality constant is independent of λ and c_j for $j = 1, \dots, A$, but dependent on K_j for $j = 1, \dots, A$.

Moreover,

$$(3.14) \quad \|p_0(t)\| \lesssim \|\varepsilon(u(t))\|_{2\mu}$$

holds.

Proof. The result follows using standard techniques. Note that the time derivative of (3.11b) reads as

$$(3.15) \quad \langle \operatorname{div} \dot{u}, q_0 \rangle - \langle \lambda^{-1} \alpha \cdot \dot{p}, q_0 \rangle = -\langle \lambda^{-1} \alpha \cdot \dot{\beta}, q_0 \rangle \quad \forall q_0 \in Q_0.$$

Taking $v = \dot{u}$ in (3.11a), $q_j = p_j$ for $1 \leq j \leq A$ in (3.11c) and $q_0 = -p_0$ in (3.15), summing the equations, and rearranging some constants (recalling that $\alpha_0 = 1$), we obtain:

$$(3.16) \quad \langle \varepsilon(u), \varepsilon(\dot{u}) \rangle_{2\mu} + \sum_{j=1}^A \langle \dot{p}_j, p_j \rangle_{c_j} + \sum_{j=1}^A \langle S_j, p_j \rangle + \sum_{j=1}^A \|\nabla p_j\|_{K_j}^2 + \langle \alpha \cdot \dot{p}, \alpha \cdot p \rangle_{\lambda^{-1}} \\ = \langle f, \dot{u} \rangle + \langle \lambda^{-1} \alpha \cdot \dot{\beta}, \alpha \cdot p \rangle + \sum_{j=1}^A \langle \gamma_j, p_j \rangle.$$

By definition (1.3), and the assumption that $\xi_{j \leftarrow i} = \xi_{i \leftarrow j}$, it follows that

$$(3.17) \quad \sum_{j=1}^A \langle S_j, p_j \rangle = \sum_{j=1}^A \sum_{i=1}^A \langle \xi_{j \leftarrow i} (p_j - p_i), p_j \rangle = \frac{1}{2} \sum_{j=1}^A \sum_{i=1}^A \|p_j - p_i\|_{\xi_{j \leftarrow i}}^2.$$

Combining (3.16) and (3.17), and pulling out the time derivatives, we find that

$$\begin{aligned} \frac{1}{2} \frac{d}{dt} \left(\|\varepsilon(u)\|_{2\mu}^2 + \sum_{j=1}^A \|p_j\|_{c_j}^2 + \|\alpha \cdot p\|_{\lambda^{-1}}^2 \right) &+ \sum_{j=1}^A \|\nabla p_j\|_{K_j}^2 + \frac{1}{2} \sum_{i,j=1}^A \|p_j - p_i\|_{\xi_{j \leftarrow i}}^2 \\ &= \langle f, \dot{u} \rangle + \langle \lambda^{-1} \alpha \cdot \dot{\beta}, \alpha \cdot p \rangle + \sum_{j=1}^A \langle \gamma_j, p_j \rangle. \end{aligned}$$

Integrating in time from 0 to t gives

$$\begin{aligned} (3.18) \quad &\|\varepsilon(u(t))\|_{2\mu}^2 + \sum_{j=1}^A \|p_j(t)\|_{c_j}^2 + \|\alpha \cdot p(t)\|_{\lambda^{-1}}^2 \\ &+ \int_0^t 2 \left[\sum_{j=1}^A \|\nabla p_j\|_{K_j}^2 + \sum_{i,j=1}^A \|p_j - p_i\|_{\xi_{j \leftarrow i}}^2 \right] ds \\ &= \|\varepsilon(u(0))\|_{2\mu}^2 + \sum_{j=1}^A \|p_j(0)\|_{c_j}^2 + \|\alpha \cdot p(0)\|_{\lambda^{-1}}^2 \\ &\quad + 2 \int_0^t \left[\langle f, \dot{u} \rangle + \langle \lambda^{-1} \alpha \cdot \dot{\beta}, \alpha \cdot p \rangle + \sum_{j=1}^A \langle \gamma_j, p_j \rangle \right] ds. \end{aligned}$$

Note first that

$$\begin{aligned} \int_0^t \langle f, \dot{u} \rangle ds &= \langle f(t), u(t) \rangle - \langle f(0), u(0) \rangle - \int_0^t \langle \dot{f}, u \rangle ds \\ &\leq \|f(t)\| \|u(t)\| + \|f(0)\| \|u(0)\| + \int_0^t \|\dot{f}\| \|u\| ds \\ &\lesssim \|f(t)\| \|\varepsilon(u(t))\|_{2\mu} + \|f(0)\| \|\varepsilon(u(0))\|_{2\mu} + \int_0^t \|\dot{f}\| \|\varepsilon(u)\|_{2\mu} ds \\ &\lesssim \frac{1}{4\epsilon_0} \|f(t)\|^2 + \epsilon_0 \|\varepsilon(u(t))\|_{2\mu}^2 + \|f(0)\| \|\varepsilon(u(0))\|_{2\mu} + \int_0^t \|\dot{f}\| \|\varepsilon(u)\|_{2\mu} ds, \end{aligned}$$

using Young's inequality (with ϵ) for any $\epsilon_0 > 0$. Again using Young's inequality with ϵ , Poincaré's inequality on Q_j and the assumption of uniform positivity of K_j on the last terms on the right hand side of (3.18), we have that for each $j = 1, \dots, A$ and any $\epsilon_j > 0$:

$$\langle \gamma_j, p_j \rangle \leq \frac{1}{4\epsilon_j} \|\gamma_j\|^2 + \epsilon_j \|p_j\|^2 \lesssim \frac{1}{4\epsilon_j} \|\gamma_j\|^2 + \epsilon_j \|\nabla p_j\|_{K_j}^2,$$

with the last inequality depending on K_j . Choosing ϵ_j for $j = 0, 1, \dots, A$ appropri-

ately and transferring terms thus give

$$\begin{aligned}
& \|\varepsilon(u(t))\|_{2\mu}^2 + \sum_{j=1}^A \|p_j(t)\|_{c_j}^2 + \|\alpha \cdot p(t)\|_{\lambda^{-1}}^2 \\
& \quad + \int_0^t \left[\sum_{j=1}^A \|\nabla p_j\|_{K_j}^2 + \sum_{i,j=1}^A \|p_j - p_i\|_{\xi_{j \leftarrow i}}^2 \right] ds \\
& \lesssim \|\varepsilon(u(0))\|_{2\mu}^2 + \|f(0)\| \|\varepsilon(u(0))\|_{2\mu} + \sum_{j=1}^A \|p_j(0)\|_{c_j}^2 + \|\alpha \cdot p(0)\|_{\lambda^{-1}}^2 + \|f(t)\|^2 \\
& \quad + \int_0^t \sum_{j=1}^A \left[\|\gamma_j\|^2 + \|\dot{f}\| \|\varepsilon(u)\|_{2\mu} + \langle \lambda^{-1} \alpha \cdot \dot{\beta}, \alpha \cdot p \rangle \right] ds.
\end{aligned}$$

Finally, the Cauchy-Schwarz inequality combined with Lemma 3.2, taking $C_1 = \|f(0)\|$, $\mathcal{G}_1(t) = \|f(t)\|^2$, and

$$\begin{aligned}
\mathcal{X}(t)^2 &= \|\varepsilon(u)\|_{2\mu}^2 + \sum_{j=1}^A \|p_j\|_{c_j}^2 + \|\alpha \cdot p\|_{\lambda^{-1}}^2 \\
& \quad + \int_0^t \left[\sum_{j=1}^A \|\nabla p_j\|_{K_j}^2 + \sum_{i,j=1}^A \|p_j - p_i\|_{\xi_{j \leftarrow i}}^2 \right] ds, \\
\mathcal{F}(s) &= \|\dot{f}(s)\| + \|\alpha \cdot \dot{\beta}(s)\|_{\lambda^{-1}}, \\
\mathcal{G}(s) &= \sum_{j=1}^A \|\gamma_j(s)\|^2,
\end{aligned}$$

give the desired estimate.

The bound for p_0 immediately follows from an inf-sup type argument: by the choice of V and Q_0 , the inf-sup condition (see e.g. [9]), by (3.6a), and Korn's inequality, we obtain that for any $t \in (0, T]$:

$$(3.19) \quad \|p_0(t)\| \lesssim \sup_{v \in V, v \neq 0} \frac{|\langle \operatorname{div} v, p_0(t) \rangle|}{\|v\|_{H^1}} = \sup_{v \in V, v \neq 0} \frac{|\langle 2\mu \varepsilon(u(t)), \varepsilon(v) \rangle|}{\|v\|_{H^1}} \lesssim \|\varepsilon(u(t))\|_{2\mu}$$

holds with constant depending on μ . \square

We remark that Theorem 3.3 gives a uniform bound on u in $L^\infty(0, T; V)$, $p_0 \in L^\infty(0, T; Q_0)$, and p_j in $L^2(0, T; Q_j)$ for $j = 1, \dots, A$, for arbitrarily large λ and arbitrarily small $c_j > 0$ for $j = 1, \dots, A$ in particular.

4. Semi-discretization of multiple network poroelasticity. In this section, we present a finite element semi-discretization of the total pressure variational formulation (3.3) of the quasi-static multiple-network poroelasticity equations. We introduce both abstract compatibility assumptions (**A1** and **A2** below) and a specific choice of conforming, mixed finite element spaces. We end this section by an *a priori* error estimate for the discretization error in the abstract case, and an *a priori* semi-discrete error estimate for a specific family of mixed finite element spaces.

4.1. Finite element semi-discretization. Let \mathcal{T}_h denote a conforming, shape-regular, simplicial discretization of Ω with discretization size $h > 0$. Relative to \mathcal{T}_h , we define finite element spaces $V_h \subset V$ and $Q_{i,h} \subset Q_i$ for $i = 0, \dots, A$. We assume that V_h and $Q_{i,h}$, $i = 0, \dots, A$ satisfy two compatibility assumptions **(A1, A2)** as follows:

A1: $V_h \times Q_{0,h}$ is a stable (in the Brezzi [11] sense) finite element pair for the Stokes equations.

A2: $Q_{j,h}$ is an H^1 -conforming finite element space for $j = 1, \dots, A$.

We also denote $Q_h = Q_{0,h} \times Q_{1,h} \times \dots \times Q_{A,h}$.

With reference to these element spaces, we define the following semi-discrete total pressure-based variational formulation of the quasi-static multiple-network poroelasticity equations: for $t \in (0, T]$, find $u_h(t) \in V_h$ and $p_{i,h}(t) \in Q_{i,h}$ for $i = 0, \dots, A$ such that

$$(4.1a) \quad \langle 2\mu\varepsilon(u_h), \varepsilon(v) \rangle + \langle p_{0,h}, \operatorname{div} v \rangle = \langle f, v \rangle \quad \forall v \in V_h,$$

$$(4.1b) \quad \langle \operatorname{div} u_h, q_0 \rangle - \langle \lambda^{-1} \alpha \cdot p_h, q_0 \rangle = 0 \quad \forall q_0 \in Q_{0,h},$$

$$(4.1c) \quad \langle c_j \dot{p}_{j,h} + \alpha_j \lambda^{-1} \alpha \cdot \dot{p}_h + S_{j,h}, q_j \rangle + \langle K_j \nabla p_{j,h}, \nabla q_j \rangle = \langle g_j, q_j \rangle \quad \forall q_j \in Q_{j,h},$$

for $j = 1, \dots, A$. Here $S_{j,h} = \sum_{i=1}^A \xi_{j \leftarrow i} (p_{j,h} - p_{i,h})$ cf. (1.3) and $p_h = (p_{0,h}, \dots, p_{A,h})$.

4.2. Auxiliary interpolation operators. As a preliminary step for the *a priori* error analysis of the semi-discrete formulation, we introduce a set of auxiliary interpolation operators. In particular, we define interpolation operators

$$\Pi_h^V : V \rightarrow V_h, \quad \Pi_h^{Q_i} : Q_i \rightarrow Q_{i,h} \quad i = 0, \dots, A,$$

as follows.

First, for any $(u, p_0) \in V \times Q_0$, we define its interpolant $(\Pi_h^V u, \Pi_h^{Q_0} p_0) \in V_h \times Q_{0,h}$ as the unique discrete solution to the Stokes-type system of equations:

$$(4.2a) \quad \langle 2\mu\varepsilon(\Pi_h^V u), \varepsilon(v) \rangle + \langle \Pi_h^{Q_0} p_0, \operatorname{div} v \rangle = \langle 2\mu\varepsilon(u), \varepsilon(v) \rangle + \langle p_0, \operatorname{div} v \rangle \quad \forall v \in V_h,$$

$$(4.2b) \quad \langle \operatorname{div} \Pi_h^V u, q_0 \rangle = \langle \operatorname{div} u, q_0 \rangle \quad \forall q_0 \in Q_{0,h}.$$

The interpolant is well-defined and bounded by assumption **A1** and the given boundary conditions.

Second, for $j = 1, \dots, A$, we define the interpolation operators $\Pi_h^{Q_j}$ as a weighted elliptic projection: i.e. for any $p_j \in Q_j$, we define its interpolant $\Pi_h^{Q_j} p_j \in Q_{j,h}$ as the unique solution of

$$(4.3) \quad \langle K_j \nabla \Pi_h^{Q_j} p_j, q \rangle = \langle K_j \nabla p_j, \nabla q \rangle \quad \forall q \in Q_{j,h}.$$

This interpolant is well-defined and bounded by assumption **A2** and the given boundary conditions.

4.3. Specific choice of finite element spaces: a family of Taylor-Hood type elements. In this paper, we will pay particular attention to one specific family of mixed finite element spaces for the total pressure-based semi-discretization of the multiple-network poroelasticity equations, namely a family of Taylor-Hood type element spaces [34, 5]. More precisely, we note that assumptions **A1** and **A2** are easily satisfied by the conforming mixed finite element space pairing:

$$(4.4) \quad V_h = \mathring{P}_{l+1}^d(\mathcal{T}_h), \quad Q_{0,h} = \mathcal{P}_l(\mathcal{T}_h), \quad Q_{j,h} = \mathring{P}_{l_j}(\mathcal{T}_h),$$

for polynomial degrees $l \geq 1$ and $l_j \geq 1$ for $j = 1, \dots, A$. We will refer to the spaces (4.4) as Taylor-Hood type elements of order l and l_j . The superimposed ring in (4.4) denotes the restriction of the piecewise polynomial spaces to conform to the given essential boundary conditions.

For this choice of finite element spaces, in particular, for the Taylor-Hood elements of order l , the following error estimate holds for the Stokes-type interpolant defined by (4.2) (see e.g. [12, 7, 8]). For $1 \leq m \leq l + 1$, if $u \in H_{0,\Gamma_D}^{m+1}(\Omega)$ and $p_0 \in H^m$, then

$$(4.5) \quad \|u - \Pi_h^V u\|_{H^1} + \|p_0 - \Pi_h^{Q_0} p_0\| \lesssim h^m (\|u\|_{H^{m+1}} + \|p_0\|_{H^m}).$$

Moreover, the following error estimate holds for the elliptic interpolants defined by (4.3) (see e.g. [10, Chap. 5]): For $j = 1, \dots, A$, for $1 \leq m \leq l_j$, if $p_j \in H_0^{m+1}$, it holds that

$$(4.6) \quad \|p_j - \Pi_h^{Q_j} p_j\|_{H^1} \lesssim h^m \|p_j\|_{H^{m+1}},$$

and under the full elliptic regularity assumption of Ω ,

$$(4.7) \quad \|p_j - \Pi_h^{Q_j} p_j\| \lesssim h^{m+1} \|p_j\|_{H^{m+1}}.$$

In the next subsection, we show optimal error estimates of semi-discrete solutions assuming that both of the above estimates hold.

4.4. Semi-discrete *a priori* error analysis. Assume that (u, p) is a solution of the continuous quasi-static multiple-network poroelasticity equations (3.6) and that (u_h, p_h) solves the corresponding semi-discrete problem (4.1). We introduce the semi-discrete (approximation) errors

$$(4.8) \quad e_u(t) \equiv u(t) - u_h(t), \quad e_{p_j}(t) \equiv p_j(t) - p_{j,h}(t) \quad j = 0, \dots, A,$$

and denote $e_p = (e_{p_0}, \dots, e_{p_A})$. We also introduce the standard decomposition of the errors into interpolation (superscript I) and discretization (superscript h) errors:

$$(4.9a) \quad e_u \equiv e_u^I + e_u^h, \quad e_u^I \equiv u - \Pi_h^V u, \quad e_u^h \equiv \Pi_h^V u - u_h,$$

$$(4.9b) \quad e_{p_j} \equiv e_{p_j}^I + e_{p_j}^h, \quad e_{p_j}^I \equiv p_j - \Pi_h^{Q_j} p_j, \quad e_{p_j}^h \equiv \Pi_h^{Q_j} p_j - p_{j,h} \quad j = 0, \dots, A.$$

Proposition 4.1 below provides estimates for the discretization errors that are robust with respect to c_j and λ . In particular, the implicit constants in the estimates are uniformly bounded for arbitrarily large λ and arbitrarily small $c_j > 0$ for $j = 1, \dots, A$. We also note that the discretization errors of u in the $L^\infty(0, T; V)$ -norm and p_j in the $L^2(0, T; Q_j)$ -norms for $j = 1, \dots, A$ converge at a higher rate than the corresponding interpolation errors, as the discretization errors are bounded essentially by the initial discretization error of u in the V -norm, by the initial discretization error of p_i in the L^2 -norm for $i = 0, \dots, A$ and by the interpolation error of p_i in the $L^2(0, T; L^2)$ -norm.

PROPOSITION 4.1. *Assume that $(u, p) \in C^1(0, T; V) \times C^1(0, T; Q)$ solves the total pressure-based variational formulation of the MPET equations (3.6) for given f and g_j for $j = 1, \dots, A$. Assume that $V_h \times Q_h$ satisfies assumptions **A1-A2**, that $(u_h, p_h) \in C^1(0, T; V_h) \times C^1(0, T; Q_h)$ solves the corresponding finite element semi-discrete problem (4.1), and that the discretization errors e_u^h and e_p^h are defined by (4.9).*

Then, the following estimate holds for all $t \in (0, T]$:

$$\begin{aligned}
 (4.10) \quad & \|\varepsilon(e_u^h(t))\|_{2\mu} + \sum_{j=1}^A \|e_{p_j}^h(t)\|_{c_j} + \|\alpha \cdot e_p^h(t)\|_{\lambda^{-1}} \\
 & + \left(\int_0^t \sum_{j=1}^A \|\nabla e_{p_j}^h\|_{K_j}^2 + \sum_{i,j=1}^A \|e_{p_j}^h - e_{p_i}^h\|_{\xi_{j \leftarrow i}}^2 ds \right)^{\frac{1}{2}} \\
 & \lesssim E_0^h + \int_0^t \|\alpha \cdot e_p^I\|_{\lambda^{-1}} ds + \left(\int_0^t \sum_{j=1}^A \|c_j \dot{e}_{p_j}^I + S_j(e_p^I)\|^2 ds \right)^{\frac{1}{2}},
 \end{aligned}$$

with an implicit constant independent of h , T , λ , c_j and $\xi_{j \leftarrow i}$ for $i, j = 1, \dots, A$ where $S_j(e_p) = \sum_{i=1}^A \xi_{j \leftarrow i}(e_{p_j} - e_{p_i})$ and

$$(4.11) \quad E_0^h = \|\varepsilon(e_u^h(0))\|_{2\mu} + \sum_{j=1}^A \|e_{p_j}^h(0)\|_{c_j} + \|\alpha \cdot e_p^h(0)\|_{\lambda^{-1}}.$$

Moreover, for $t \in (0, T]$,

$$(4.12) \quad \|e_{p_0}^h(t)\| \lesssim \|\varepsilon(e_u^h(t))\|_{2\mu}.$$

Proof. A standard subtraction of (4.1) from (3.6) gives that the errors e_u and e_p satisfy the error equations:

$$(4.13a) \quad \langle 2\mu \varepsilon(e_u), \varepsilon(v) \rangle + \langle e_{p_0}, \operatorname{div} v \rangle = 0 \quad \forall v \in V_h,$$

$$(4.13b) \quad \langle \operatorname{div} e_u, q_0 \rangle - \langle \lambda^{-1} \alpha \cdot e_p, q_0 \rangle = 0 \quad \forall q_0 \in Q_{0,h},$$

$$(4.13c) \quad \langle c_j \dot{e}_{p_j} + \alpha_j \lambda^{-1} \alpha \cdot \dot{e}_p + S_j(e_p), q_j \rangle + \langle K_j \nabla e_{p_j}, \nabla q_j \rangle = 0 \quad \forall q_j \in Q_{j,h},$$

for $j = 1, \dots, A$ with $S_j(e_p) = \sum_{i=1}^A \xi_{j \leftarrow i}(e_{p_j} - e_{p_i})$. By the definition of the interpolation operators Π_h , we obtain the reduced error representations:

$$(4.14a) \quad \langle 2\mu \varepsilon(e_u^h), \varepsilon(v) \rangle + \langle e_{p_0}^h, \operatorname{div} v \rangle = 0 \quad \forall v \in V_h,$$

$$(4.14b) \quad \langle \operatorname{div} e_u^h, q_0 \rangle - \langle \lambda^{-1} \alpha \cdot e_p^h, q_0 \rangle = \langle g_0^I, q_0 \rangle \quad \forall q_0 \in Q_{0,h},$$

$$(4.14c) \quad \langle c_j \dot{e}_{p_j}^h + \alpha_j \lambda^{-1} \alpha \cdot \dot{e}_p^h + S_j(e_p^h), q_j \rangle + \langle K_j \nabla e_{p_j}^h, \nabla q_j \rangle = \langle g_j^I, q_j \rangle \quad \forall q_j \in Q_{j,h},$$

for $j = 1, \dots, A$ where $g_0^I = \lambda^{-1} \alpha \cdot e_p^I$ and $g_j^I = -c_j \dot{e}_{p_j}^I - \alpha_j \lambda^{-1} \alpha \cdot \dot{e}_p^I - S_j(e_p^I)$. Noting that e_u^h and e_p^h satisfy the assumptions of Theorem 3.3 with $f = 0$, $\beta = -e_p^I$ and $\gamma_j = -c_j \dot{e}_{p_j}^I - S_j(e_p^I)$, the semi-discrete discretization error estimate (4.10) follows.

Further, by the same techniques as used for the bound (3.14), and assumption **A1** combined with (4.14a), we observe that

$$(4.15) \quad \|e_{p_0}^h(t)\| \lesssim \sup_{v \in V_h, v \neq 0} \frac{|\langle \operatorname{div} v, e_{p_0}^h(t) \rangle|}{\|v\|_{H^1}} = \sup_{v \in V_h, v \neq 0} \frac{|\langle 2\mu \varepsilon(e_u^h(t)), \varepsilon(v) \rangle|}{\|v\|_{H^1}} \lesssim \|\varepsilon(e_u^h(t))\|_{2\mu},$$

with constant depending on μ , thus yielding (4.12). \square

We now consider error estimates associated with the specific choice of Taylor-Hood type finite element spaces as introduced in Section 4.3. Theorem 4.2 below presents a complete semi-discrete error estimate for this case, and is easily extendable to other elements satisfying **A1** and **A2**.

THEOREM 4.2. Assume that (u, p) and (u_h, p_h) are defined as in Proposition 4.1 over Taylor-Hood type elements of order l and l_j for $j = 1, \dots, A$ as defined by (4.4), and that (e_u, e_p) is defined by (4.8). Assume that (u, p) is sufficiently regular. Then the following three estimates hold for all $t \in (0, T]$ with implicit constants independent of h , T , λ , c_j and $\xi_{j \leftarrow i}$ for $i, j = 1, \dots, A$. First,

$$(4.16) \quad \begin{aligned} \|u(t) - u_h(t)\|_{H^1} &\lesssim E_0^h + h^{l+1} (\|u(t)\|_{H^{l+2}} + \|u\|_{L^1(0,t;H^{l+2})} + \|p_0\|_{L^1(0,t;H^{l+1})}) \\ &\quad + \sum_{j=1}^A h^{l_j+1} (\|p_j\|_{L^1(0,t;H^{l_j+1})} + \|\dot{p}_j, p_j\|_{L^2(0,t;H^{l_j+1})}), \end{aligned}$$

holds with E_0^h defined in (4.11), and

$$\|\dot{p}_j, p_j\|_{L^2(0,t;H^{l_j+1})} \equiv \|\dot{p}_j\|_{L^2(0,t;H^{l_j+1})} + \|p_j\|_{L^2(0,t;H^{l_j+1})}.$$

In addition,

$$(4.17) \quad \begin{aligned} \sum_{j=1}^A \|p_j - p_{j,h}\|_{L^2(0,t;H^1)} &\lesssim E_0^h + h^{l+1} (\|u\|_{L^1(0,t;H^{l+2})} + \|p_0\|_{L^1(0,t;H^{l+1})}) \\ &\quad + \sum_{j=1}^A h^{l_j} \|p_j\|_{L^2(0,t;H^{l_j+1})} + h^{l_j+1} (\|p_j\|_{L^1(0,t;H^{l_j+1})} + \|\dot{p}_j, p_j\|_{L^2(0,t;H^{l_j+1})}) \end{aligned}$$

and

$$(4.18) \quad \|p_0(t) - p_{0,h}(t)\| \lesssim h^{l+1} (\|p_0(t)\|_{H^{l+1}} + \|u(t)\|_{H^{l+2}}) + \|\varepsilon(e_u^h(t))\|_{2\mu}$$

hold.

Proof. Let (u, p) , (u_h, p_h) and (e_u, e_p) be as stated. By the triangle inequality, the definition of e_u^h , Korn's inequality, and (4.5) for any $t \in (0, T]$, we have that

$$\begin{aligned} \|u(t) - u_h(t)\|_{H^1} &\leq \|u(t) - \Pi_h^V u(t)\|_{H^1} + \|\Pi_h^V u(t) - u_h(t)\|_{H^1} \\ &\lesssim h^{l+1} \|u(t)\|_{H^{l+2}} + \|\varepsilon(e_u^h(t))\|_{2\mu}, \end{aligned}$$

with inequality constant depending on Ω and μ . Further, Proposition 4.1 gives for any $t \in (0, T]$ that

$$(4.19) \quad \|\varepsilon(e_u^h(t))\|_{2\mu} \lesssim E_0^h + \int_0^t \|\alpha \cdot e_p^I\|_{\lambda^{-1}} ds + \left(\int_0^t \sum_{j=1}^A \|c_j \dot{e}_{p_j}^I + S_j(e_p^I)\|^2 ds \right)^{\frac{1}{2}},$$

where E_0^h is defined by (4.11). Applying (4.5) and (4.7), we note that for any $t \in (0, T]$

$$(4.20) \quad \|\alpha \cdot e_p^I(t)\|_{\lambda^{-1}} \lesssim h^{l+1} (\|u(t)\|_{H^{l+2}} + \|p_0(t)\|_{H^{l+1}}) + \sum_{j=1}^A h^{l_j+1} \|p_j(t)\|_{H^{l_j+1}}.$$

Similarly, by (4.7) and the definition of S_j , we have that

$$(4.21) \quad \sum_{j=1}^A \|c_j \dot{e}_{p_j}^I(t) + S_j(e_p^I(t))\| \lesssim \sum_{j=1}^A h^{l_j+1} \|\dot{p}_j(t)\|_{H^{l_j+1}} + h^{l_j+1} \|p_j(t)\|_{H^{l_j+1}}.$$

Combining the above estimates and rearranging terms yield (4.16).

Turning to the pressures p_j , analogously using the triangle inequality, (4.6), the Poincaré inequality, and the assumptions on K_j , we have for any $t \in (0, T]$ and any $j = 1, \dots, A$ that

$$\begin{aligned} \|p_j - p_{j,h}\|_{L^2(0,t;H^1)} &\leq \|p_j - \Pi_h^{Q_j} p_j\|_{L^2(0,t;H^1)} + \|\Pi_h^{Q_j} p_j - p_{j,h}\|_{L^2(0,t;H^1)} \\ &\lesssim h^{l_j} \|p_j\|_{L^2(0,t;H^{l_j+1})} + \left(\int_0^t \|\nabla e_{p_j}^h(s)\|_{K_j}^2 ds \right)^{\frac{1}{2}}, \end{aligned}$$

where the constant in the second inequality depends on Ω and the lower bound on K_j . Using Proposition 4.1 together with (4.20) and (4.21), we thus obtain the estimate given by (4.17).

Finally, (4.18) follows from

$$\|p_0(t) - p_{0,h}(t)\| \leq \|p_0(t) - \Pi_h^{Q_0} p_0(t)\| + \|\Pi_h^{Q_0} p_0(t) - p_{0,h}(t)\|,$$

(4.5), and (4.12). \square

REMARK 4.3. We remark that the estimates of Theorem 3.3, Proposition 4.1, and Theorem 4.2 all hold uniformly as $c_j \rightarrow 0$, including in the case $c_j = 0$, for any $j = 1, \dots, A$.

Theorem 4.2 above provides an optimal estimate for p_j in the $L^\infty(0, t; H^1)$ -norm for $j = 1, \dots, A$. Moreover, Proposition 4.1 also yields an optimal estimate for p_j in the $L^\infty(0, t; L^2)$ -norm for $j = 1, \dots, A$, as summarized in Proposition 4.4 below.

PROPOSITION 4.4. Let (u, p) , (u_h, p_h) , (e_u, e_p) be as in Theorem 4.2 and let $c_j > 0$ for $j = 1, \dots, A$. Then, the following estimate holds for all $t \in (0, T]$ with implicit constant independent of h , T , λ and $\xi_{j \leftarrow i} \geq 0$ for any $i, j = 1, \dots, A$:

$$\begin{aligned} (4.22) \quad \sum_{j=1}^A \|e_{p_j}(t)\| &\lesssim E_0^h + h^{l+1} (\|u\|_{L^1(0,t;H^{l+2})} + \|p_0\|_{L^1(0,t;H^{l+1})}) \\ &+ \sum_{j=1}^A h^{l_j+1} \left(\|p_j\|_{H^{l_j+1}} + \|p_j\|_{L^1(0,t;H^{l_j+1})} + \|p_j\|_{L^2(0,t;H^{l_j+1})} + \|\dot{p}_j\|_{L^2(0,t;H^{l_j+1})} \right) \end{aligned}$$

with E_0^h in (4.11).

Proof. Using the triangle inequality and (4.7), we find that

$$(4.23) \quad \sum_{j=1}^A \|e_{p_j}\| \leq \sum_{j=1}^A \|e_{p_j}^I\| + \|e_{p_j}^h\| \lesssim \sum_{j=1}^A h^{l_j+1} \|p_j\|_{H^{l_j+1}} + \|e_{p_j}^h\|.$$

Further, using Proposition 4.1 and the assumption that $c_j > 0$ for all j , (4.20), and (4.21), we obtain (4.22). \square

5. Numerical convergence experiments. In this section, we present a set of numerical examples to illustrate the theoretical results presented. In particular, we examine the convergence of the numerical approximations for test cases with smooth solutions. All numerical simulations in this section and in the subsequent Section 6 were run using the FEniCS finite element software [3] (version 2018.1+), and the simulation and post-processing code is openly available [30].

h	$\ u(T) - u_h(T)\ $	Rate	$\ u(T) - u_h(T)\ _{H^1}$	Rate
H	3.13×10^{-2}		7.28×10^{-1}	
$H/2$	3.64×10^{-3}	3.11	1.98×10^{-1}	1.88
$H/4$	4.35×10^{-4}	3.06	5.06×10^{-2}	1.96
$H/8$	5.36×10^{-5}	3.02	1.27×10^{-2}	1.99
$H/16$	6.67×10^{-6}	3.01	3.19×10^{-3}	2.00
Optimal		3		2

h	$\ p_1(T) - p_{1,h}(T)\ $	Rate	$\ p_1(T) - p_{1,h}(T)\ _{H^1}$	Rate
H	3.69×10^{-2}		4.21×10^{-1}	
$H/2$	9.57×10^{-3}	1.92	2.16×10^{-1}	0.96
$H/4$	2.47×10^{-3}	1.98	1.09×10^{-1}	0.99
$H/8$	6.21×10^{-4}	1.99	5.45×10^{-2}	1.00
$H/16$	1.55×10^{-4}	2.00	2.73×10^{-2}	1.00
Optimal		2		1

h	$\ p_0(T) - p_{0,h}(T)\ $	Rate
H	1.42×10^{-1}	
$H/2$	3.10×10^{-2}	2.19
$H/4$	7.56×10^{-3}	2.04
$H/8$	1.88×10^{-3}	2.01
$H/16$	4.70×10^{-4}	2.00
Optimal		2

Table 2: Approximation errors and convergence rates for the total pressure-based mixed finite element discretization for the smooth manufactured test case for a nearly incompressible material introduced in Example 1.1. We observe that the optimal convergence is restored for the total pressure-based scheme. This is in contrast to the sub-optimal rates observed with the standard scheme (cf. Table 1). The coarsest mesh size H corresponds to a uniform mesh constructed by dividing the unit square into 4×4 squares and dividing each square by a diagonal.

5.1. Convergence in the nearly incompressible case. We consider the manufactured solution test case introduced in Example 1.1. As before, we consider a series of uniform meshes of the computational domain. The coarsest mesh size H corresponds to a uniform mesh constructed by dividing the unit square into 4×4 squares and dividing each square by a diagonal.

We let $V_h \times Q_h$ be the lowest-order Taylor-Hood-type elements, as defined by (4.4) with $l = 1$ and $l_j = 1$ for $j = 1, \dots, A$, for the semi-discrete total pressure variational formulation (4.1). For this experiment, we used a Crank-Nicolson discretization in time with time step size $\Delta t = 0.125$ and $T = 0.5$. Since the exact solutions are linear in time, we expected this choice of temporal discretization to be exact. Indeed, we tested with multiple time step sizes and found that the errors did not depend on the time step size.

We computed the approximation error of $u_h(T)$ and $p_h(T)$ in the L^2 and H^1 -

norms. The resulting errors for u_h , $p_{0,h}$, and $p_{1,h}$ are presented in Table 2, together with computed convergence rates. The errors and convergence rates of $p_{2,h}$ were comparable and analogous to those of $p_{1,h}$ and, for this reason, not reported here.

From Theorem 4.2 and Proposition 4.4, we expect second order convergence (with decreasing mesh size h) for $u(T)$ in the H^1 -norm, second order convergence for $p_0(T)$ in the L^2 -norm, first order convergence for $p_j(T)$ in the H^1 -norm and second order convergence for $p_j(T)$ in the L^2 -norm (since $c_j > 0$) for $j = 1, \dots, A$. The numerically computed errors are in agreement with these theoretical results. In particular, we recover the optimal convergence rates of 2 for u_h in the H^1 -norm, 2 for p_j in the L^2 -norm and 1 for p_j in the H^1 -norm.

Additionally, we observe that we recover the optimal convergence rate of 3 for $u_h(T)$ in the L^2 -norm for this test case. Further investigations indicate that this does not hold for general ν : with $\nu = 0.4$, the convergence rate for $u_h(T)$ in the L^2 -norm is reduced to between 2 and 3, cf. Table 3.

h	$\ u(T) - u_h(T)\ $	Rate	$\ u(T) - u_h(T)\ _{H^1}$	Rate
H	3.12×10^{-2}		7.25×10^0	
$H/2$	3.86×10^{-3}	3.02	1.98×10^{-1}	1.87
$H/4$	5.47×10^{-4}	2.82	5.08×10^{-2}	1.96
$H/8$	9.90×10^{-5}	2.47	1.28×10^{-2}	1.99
$H/16$	2.19×10^{-5}	2.18	3.20×10^{-3}	2.00

Table 3: Displacement approximation errors and convergence rates for the total pressure-based mixed finite element discretization for the smooth manufactured test case introduced in Example 1.1 but with $\nu = 0.4$. The coarsest mesh size H corresponds to a uniform mesh constructed by dividing the unit square into 4×4 squares and dividing each square by a diagonal. We note that the third order convergence rate for $u_h(T)$ in the L^2 -norm observed in Table 3 is reduced to order 2 – 3 in this case with $\nu = 0.4$.

5.2. Convergence in the vanishing storage coefficient case. We also considered the same test case, total-pressure-based discretization, and set-up as described in Section 5.1, but now with $c_j = 0$ for $j = 1, 2$. The corresponding errors are presented in Table 4. We note that we observe the same optimal convergence rates as before for this case with $c_j = 0$.

5.3. Convergence of the discretization error. Proposition 4.1 indicates superconvergence of the discretization errors e_u^h and $e_{p_j}^h$. In particular, this result predicts that for the lowest-order Taylor-Hood-type elements, we expect to observe second order convergence for the discretization error of p_j in the $L^2(0, T; H^1)$ -norm. To examine this numerically, we consider the same test case, total-pressure-based discretization, and set-up as described in Section 5.1, but now compute the error between the elliptic interpolants and the finite element approximation. The results are given in Table 5 for p_1 . The numerical results were entirely analogous for p_2 and therefore not shown. We indeed observe the second order convergence of $e_{p_j}^h(T)$ (for $j = 1, 2$) in the H^1 -norm as indicated by Proposition 4.1.

h	$\ u(T) - u_h(T)\ $	Rate	$\ u(T) - u_h(T)\ _{H^1}$	Rate
H	3.13×10^{-2}		7.28×10^{-1}	
$H/2$	3.64×10^{-3}	3.11	1.98×10^{-1}	1.88
$H/4$	4.35×10^{-4}	3.06	5.06×10^{-2}	1.96
$H/8$	5.36×10^{-5}	3.02	1.27×10^{-2}	1.99
$H/16$	6.67×10^{-6}	3.01	3.19×10^{-3}	2.00
Optimal		3		2

h	$\ p_1(T) - p_{1,h}(T)\ $	Rate	$\ p_1(T) - p_{1,h}(T)\ _{H^1}$	Rate
H	3.95×10^{-2}		4.21×10^{-1}	
$H/2$	1.06×10^{-2}	1.90	2.16×10^{-1}	0.96
$H/4$	2.69×10^{-3}	1.97	1.09×10^{-1}	0.99
$H/8$	6.75×10^{-4}	1.99	5.45×10^{-2}	1.00
$H/16$	1.69×10^{-4}	2.00	2.73×10^{-2}	1.00
Optimal		2		1

h	$\ p_0(T) - p_{0,h}(T)\ $	Rate
H	1.46×10^{-1}	
$H/2$	3.25×10^{-2}	2.17
$H/4$	7.97×10^{-3}	2.03
$H/8$	1.99×10^{-3}	2.00
$H/16$	4.96×10^{-4}	2.00
Optimal		2

Table 4: Approximation errors and convergence rates for the total pressure-based mixed finite element discretization for the smooth manufactured test case introduced in Example 1.1 but with vanishing storage coefficients ($c_j = 0$ for $j = 1, 2$). We observe the optimal convergence also for this set of parameter values. The coarsest mesh size H corresponds to a uniform mesh constructed by dividing the unit square into 4×4 squares and dividing each square by a diagonal.

6. Simulating fluid flow and displacement in a human brain using a 4-network model. In this section, we consider a variant of the 4-network model presented in [35] defined over a human brain mesh with physiologically inspired parameters and boundary conditions. In particular, we consider the MPET equations (1.1) with $A = 4$. The original 4 networks of [35] represent (1) interstitial fluid-filled extracellular spaces, (2) arteries, (3) veins and (4) capillaries. In view of recent findings [1] however, we conjecture that it may be more physiologically interesting to interpret the extracellular compartment as a paravascular network.

The computational domain is defined by Version 2 of the Colin 27 Adult Brain Atlas FEM mesh [15], in particular a coarsened version of this mesh with 99 605 cells and 29 037 vertices, and is illustrated in Figure 1 (left). The domain boundary consists of the outer surface of the brain, referred to below as the *skull*, and of inner convexities, referred to as the *ventricles*, cf. Figure 1 (right). We selected three points in the domain $x_0 = (89.9, 108.9, 82.3)$ (center), $x_1 = (102.2, 139.3, 82.3)$ (point in the

h	$\ \Pi_h^1 p_1(T) - p_{1,h}(T)\ $	Rate	$\ \Pi_h^1 p_1(T) - p_{1,h}(T)\ _{H^1}$	Rate
H	2.98×10^{-3}		1.46×10^{-2}	
$H/2$	9.12×10^{-4}	1.71	4.25×10^{-2}	1.78
$H/4$	2.40×10^{-4}	1.92	1.11×10^{-2}	1.94
$H/8$	6.09×10^{-5}	1.98	2.79×10^{-2}	1.99
$H/16$	1.53×10^{-5}	2.00	6.99×10^{-2}	2.00
Theoretical		2		2

Table 5: Discretization errors and convergence rates for p_1 for the total pressure-based mixed finite element discretization for the smooth manufactured test case for a nearly incompressible material introduced in Example 1.1. We indeed observe the higher (second) order convergence of $e_{p_1}^h(T)$ in the H^1 -norm as indicated by Proposition 4.1. The coarsest mesh size H corresponds to a uniform mesh constructed by dividing the unit square into 4×4 squares and dividing each square by a diagonal.

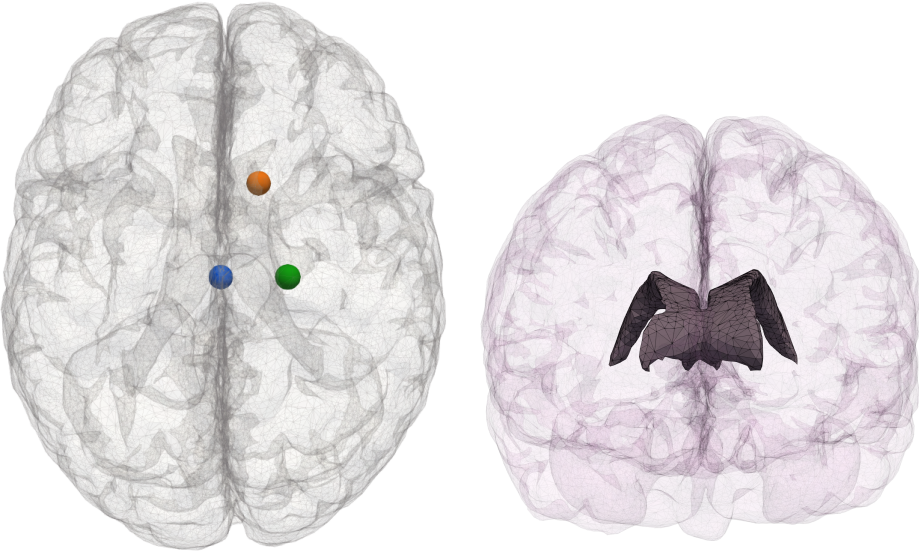


Fig. 1: Left: The human brain computational mesh used in Section 6 with 99 605 cells and 29 037 vertices. View from top i.e. along the negative z-axis. The points x_0 (blue), x_1 (orange), x_2 (green) are marked with spheres. Right: The inner (ventricular) boundaries of the computational mesh. View from front i.e. along negative y-axis.

central z-plane), and $x_2 = (110.7, 108.9, 98.5)$ (point in the central y-plane). The relative locations of these points within the domain are also illustrated in Figure 1 (left).

We consider the following set of boundary conditions for the system for all $t \in (0, T)$. All boundary pressure values are given in mmHg below, noting that 1 mmHg

Symbol	Value(s)	Units	Reference
ν	0.4999		Comparable with [26]
E	1500	Pa	Comparable with [13]
c_1	3.9×10^{-4}	Pa^{-1}	[16, Table 2]
c_2, c_4	2.9×10^{-4}	Pa^{-1}	[16, Table 2]
c_3	1.5×10^{-5}	Pa^{-1}	[16, Table 2]
α_1	0.49		[16, Table 2]
α_2, α_4	0.25		[16, Table 2]
α_3	0.01		[16, Table 2]
K_1	$1.57 \cdot 10^{-5}$	$\text{mm}^2 \text{ Pa}^{-1} \text{ s}^{-1}$	[36, Table 1]
$K_2, K_3, K_4,$	$3.75 \cdot 10^{-2}$	$\text{mm}^2 \text{ Pa}^{-1} \text{ s}^{-1}$	[36, Table 1]
$\xi_{2 \leftarrow 4}, \xi_{4 \leftarrow 3}, \xi_{4 \leftarrow 1}, \xi_{1 \leftarrow 3}$	1.0×10^{-6}	$\text{Pa}^{-1} \text{ s}^{-1}$	Comparable with [24]
$\xi_{1 \leftarrow 2}, \xi_{2 \leftarrow 3}$	0.0	$\text{Pa}^{-1} \text{ s}^{-1}$	[36]

Table 6: Material parameters used for the multiple network poroelasticity equations (1.1) with $A = 4$ networks for the numerical experiments in Section 6. We remark that a wide range of parameter values can be found in the literature and the ones used here represents one sample set of representative values.

≈ 133.32 Pa. We assume that the displacement is fixed on the outer boundary and prescribe a total stress on the inner boundary:

$$u = 0 \quad \text{on skull}, \quad (C\varepsilon(u) - \sum_{j=1}^4 \alpha_j p_j I) \cdot n = s n \quad \text{on ventricles},$$

where n is the outward boundary normal and s is defined as

$$s = - \sum_{j=1}^4 \alpha_j \tilde{p}_j,$$

where \tilde{p}_j for $j = 1, \dots, 4$ are given below. We assume that the fluid in network 1 is in direct communication with the surrounding cerebrospinal fluid, and that a cerebrospinal fluid pressure is prescribed. In particular, we assume that the cerebrospinal fluid pressure pulsates around a baseline pressure of 5 (mmHg) with a peak transmantle pressure difference magnitude of $\delta = 0.012$ (mmHg):

$$p_1 = 5 + 2 \sin(2\pi t) \quad \text{on skull}, \quad p_1 = 5 + (2 + \delta) \sin(2\pi t) \equiv \tilde{p}_1 \quad \text{on ventricles}.$$

We assume that a pulsating arterial blood pressure is prescribed at the outer boundary, while on the inner boundaries, we assume no arterial flux:

$$p_2 = 70 + 10 \sin(2\pi t) \equiv \tilde{p}_2 \quad \text{on skull}, \quad \nabla p_2 \cdot n = 0 \quad \text{on ventricles}.$$

For the venous compartment, we assume that a constant pressure is prescribed at both boundaries:

$$p_3 = 6 \equiv \tilde{p}_3 \quad \text{on skull and ventricles}.$$

Finally, for the capillary compartment, we assume no flux at both boundaries:

$$\nabla p_4 \cdot n = 0 \quad \text{on skull and ventricles.}$$

We consider the following initial conditions:

$$u = 0, \quad p_1 = 5, \quad p_2 = 70, \quad p_3 = 6, \quad p_4 = (p_2 + p_3)/2 \equiv \tilde{p}_4,$$

and material parameters as reported in Table 6.

We computed the resulting solutions using the total pressure mixed finite element formulation with the lowest order Taylor-Hood type elements ($l = 1$ and $l_j = 1$ for $j = 1, \dots, 4$ in (4.4)), a Crank-Nicolson type discretization in time with time step $\Delta t = 0.0125$ (s) over the time interval $(0.0, 3.0)$ (s). The linear systems of equations were solved using a direct solver (MUMPS). For comparison, we also computed solutions with a standard mixed finite element formulation (as described and used in Example 1.1) and otherwise the same numerical set-up.

The numerical results using the total pressure formulation are presented in Figures 2 and 3. In particular, snapshots of the displacement and network pressures at peak arterial inflow in the 3rd cycle ($t = 2.25$ (s)) are presented in Figure 2. Plots of the displacement magnitude and network pressures in a set of points versus time are presented in Figure 3.

We also compared the solutions computed using the total pressure and standard mixed finite element formulation. Plots of the displacement magnitude in a set of points over time are presented in Figure 4. We clearly observe that the computed displacements using the two formulations differ. For instance, the displacement magnitude in the point x_0 computed using the standard formulation is less than half the magnitude computed using the total pressure formulation. We also visually compared the pressures computed using the two formulations and found only minimal differences for this test case (data not shown for the standard formulation).

7. Conclusions. In this paper, we have presented a new mixed finite element formulation for the quasi-static multiple-network poroelasticity equations. Our formulation introduces a single additional scalar field unknown, the total pressure. We prove, via energy and semi-discrete *a priori* error estimates, that this formulation is robust in the limits of incompressibility ($\lambda \rightarrow \infty$) and vanishing storage coefficients ($c_j \rightarrow 0$), in contrast to standard formulations. Finally, numerical experiments support the theoretical results. For the numerical experiments presented here, we have used direct linear solvers. In future work, we will address iterative solvers and preconditioning of the MPET equations.

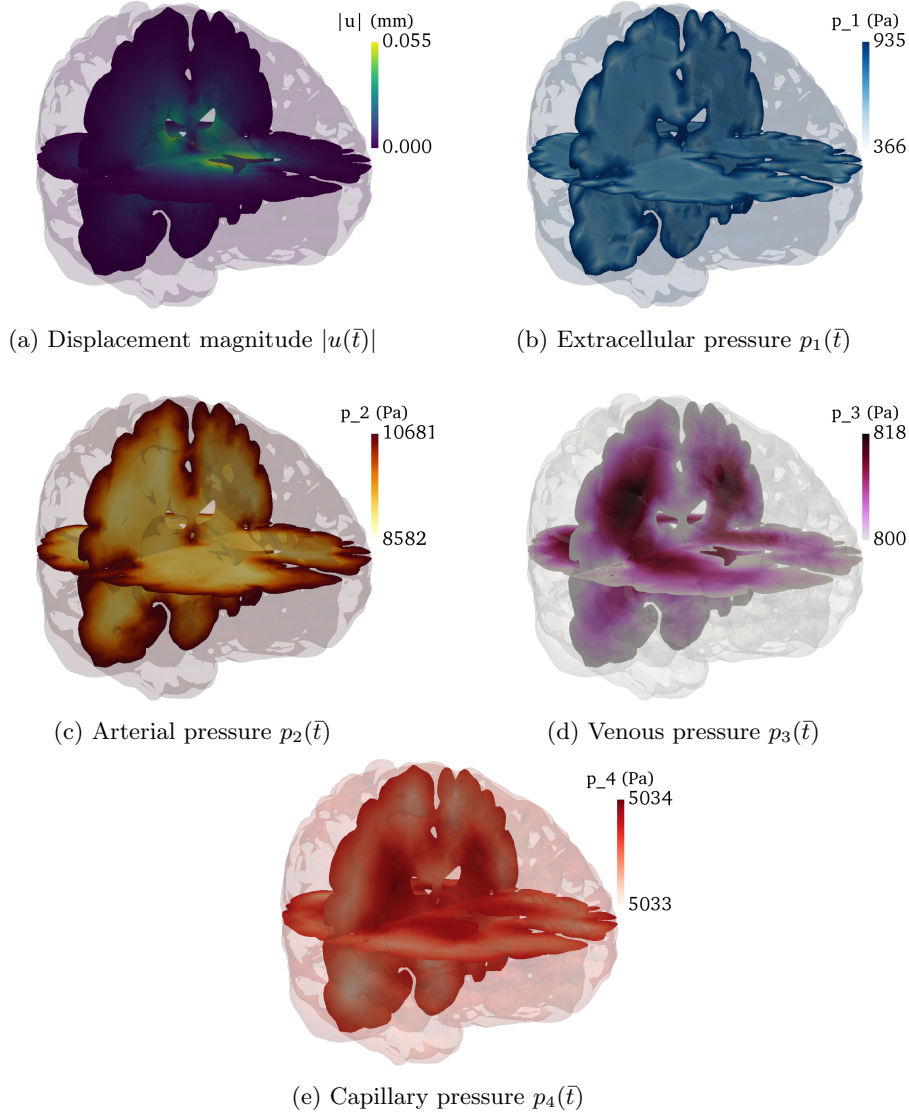


Fig. 2: Results of numerical experiment described in Section 6 using the total pressure formulation. Plots show slices of computed quantities at $\bar{t} = 2.25$ (s) corresponding to the peak arterial inflow in the 2nd cycle. From left to right and top to bottom: (a) displacement magnitude $|u|$, (b) extracellular pressure p_1 , (c) arterial blood pressure p_2 , (d) venous blood pressure p_3 and (e) capillary blood pressure p_4 .

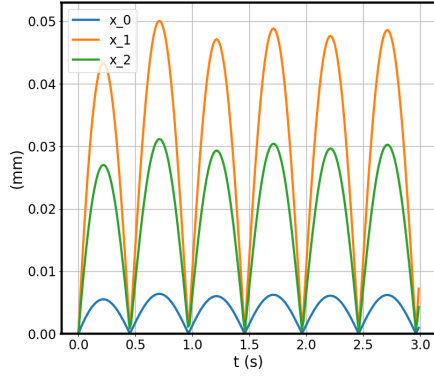
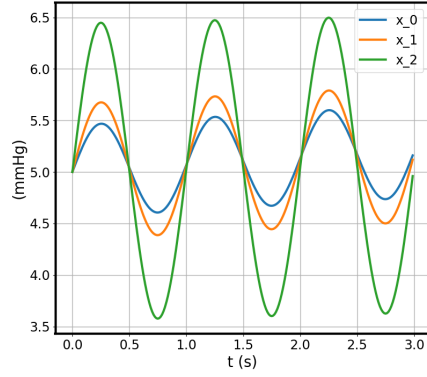
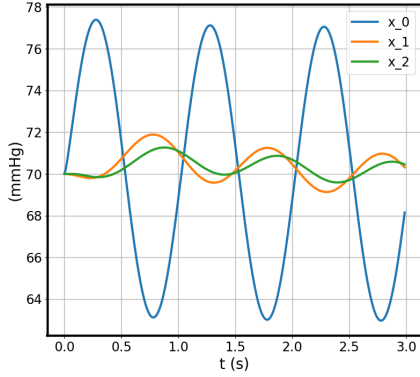
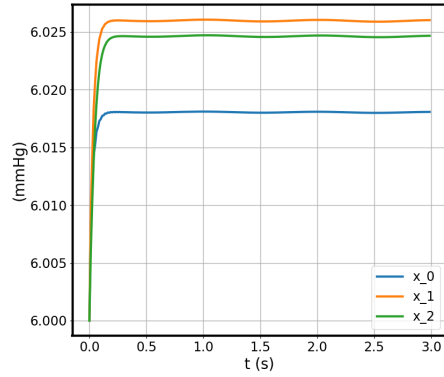
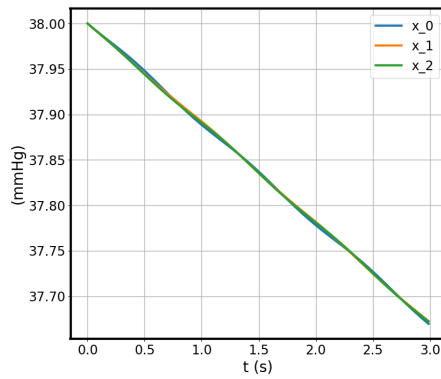
(a) Displacement magnitude $|u(x_i)|$ (b) Extracellular pressure $p_1(x_i)$ (c) Arterial pressure $p_2(x_i)$ (d) Venous pressure $p_3(x_i)$ (e) Capillary pressure $p_4(x_i)$

Fig. 3: Results of numerical experiment described in Section 6 using the total pressure formulation. Plots show computed quantities over time $t \in (0.0, 3.0)$ for a set of three points x_0, x_1, x_2 . See Figure 1 for the location and precise coordinates of the points x_i . From left to right and top to bottom: (a) displacement magnitude $|u|$, (b) extracellular pressure p_1 , (c) arterial blood pressure p_2 , (d) venous blood pressure p_3 and (e) capillary blood pressure p_4 .

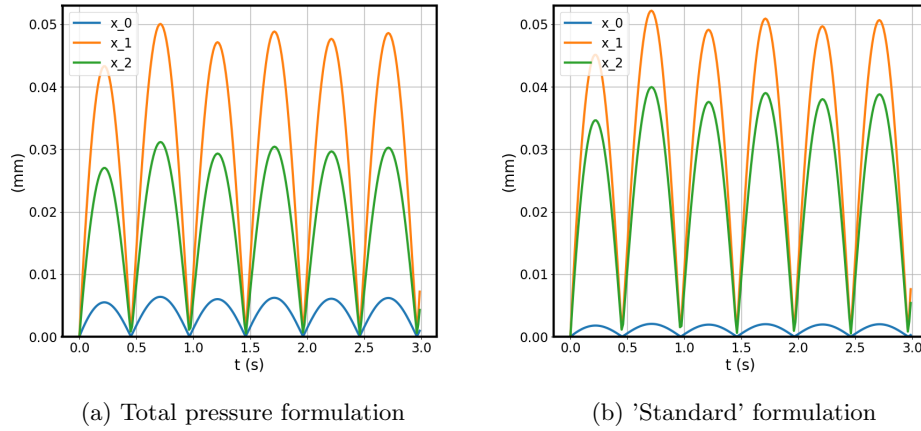


Fig. 4: Comparison of displacements computed using the standard and total pressure formulation (cf. Section 6). Plots of displacement magnitude $|u(x_i, t)|$ versus time t , for a set of points x_0, x_1, x_2 (see Figure 1 for the location and precise coordinates of the points x_i): (a) Total-pressure mixed finite element formulation, (b) Standard mixed finite element formulation (cf. Example 1.1). The computed displacements clearly differ between the two solution methods.

REFERENCES

- [1] N. J. ABBOTT, M. E. PIZZO, J. E. PRESTON, D. JANIGRO, AND R. G. THORNE, *The role of brain barriers in fluid movement in the CNS: is there a "glymphatic" system?*, *Acta Neuropathol.*, (2018), pp. 1–21.
- [2] G. AGUILAR, F. GASPAR, F. LISBONA, AND C. RODRIGO, *Numerical stabilization of Biot's consolidation model by a perturbation on the flow equation*, *Inter. J. Numer. Meth. Eng.*, 75 (2008), pp. 1282–1300.
- [3] M. ALNÆS, J. BLECHTA, J. HAKE, A. JOHANSSON, B. KEHLET, A. LOGG, C. RICHARDSON, J. RING, M. E. ROGNES, AND G. N. WELLS, *The FEniCS project version 1.5*, *Archive of Numerical Software*, 3 (2015), pp. 9–23.
- [4] M. BAUSE, F. RADU, AND U. KÖCHER, *Space-time finite element approximation of the Biot poroelasticity system with iterative coupling*, *Comput. Methods in Appl. Mech. Eng.*, 320 (2017), pp. 745–768.
- [5] M. BERCOVIER AND O. PIRONNEAU, *Error estimates for finite element method solution of the Stokes problem in the primitive variables*, *Numer. Math.*, 33 (1979), pp. 211–224, <https://doi.org/10.1007/BF01399555>.
- [6] L. BERGER, R. BORDAS, D. KAY, AND S. TAVENER, *Stabilized lowest-order finite element approximation for linear three-field poroelasticity*, *SIAM J. Sci. Comp.*, 37 (2015), pp. A2222–A2245.
- [7] D. BOFFI, *Stability of higher order triangular Hood-Taylor methods for the stationary Stokes equations*, *Math. Models Methods Appl. Sci.*, 4 (1994), pp. 223–235, <https://doi.org/10.1142/S0218202594000133>.
- [8] D. BOFFI, *Three-dimensional finite element methods for the Stokes problem*, *SIAM J. Numer. Anal.*, 34 (1997), pp. 664–670, <https://doi.org/10.1137/S0036142994270193>.
- [9] D. BRAESS, *Finite elements: Theory, fast solvers, and applications in solid mechanics (2nd edition)*, Cambridge University Press, 2001.
- [10] S. C. BRENNER AND L. R. SCOTT, *The Mathematical Theory of Finite Element Methods*, Springer, Third ed., 2008, [https://doi.org/10.1016/0022-1236\(78\)90073-3](https://doi.org/10.1016/0022-1236(78)90073-3).
- [11] F. BREZZI, *On the existence, uniqueness and approximation of saddle-point problems arising from Lagrangian multipliers*, *Rev. Française Automat. Informat. Recherche Opérationnelle Sér. Rouge*, 8 (1974), pp. 129–151.
- [12] F. BREZZI AND R. S. FALK, *Stability of higher-order Hood-Taylor methods*, *SIAM J. Numer. Anal.*, 28 (1991), pp. 581–590.
- [13] S. BUDDAY, R. NAY, R. DE ROOIJ, P. STEINMANN, T. WYROBEK, T. C. OVAERT, AND E. KUHL, *Mechanical properties of gray and white matter brain tissue by indentation*, *J. Mech. Behav. Biomed. Mater.*, 46 (2015), pp. 318–330.
- [14] L. C. EVANS, *Partial differential equations*, vol. 19 of Graduate Studies in Mathematics, American Mathematical Society, Providence, RI, 1998.
- [15] Q. FANG, *Mesh-based Monte Carlo method using fast ray-tracing in Plücker coordinates*, *Biomed. Opt. Express*, 1 (2010), pp. 165–175.
- [16] L. GUO, J. C. VARDAKIS, T. LASSILA, M. MITOLO, N. RAVIKUMAR, D. CHOU, M. LANGE, A. SARRAMI-FORUSHANI, B. J. TULLY, Z. A. TAYLOR, ET AL., *Subject-specific multiporoelastic model for exploring the risk factors associated with the early stages of Alzheimer's disease*, *Interface Focus*, 8 (2018), p. 20170019.
- [17] X. HU, C. RODRIGO, F. J. GASPAR, AND L. T. ZIKATANOV, *A nonconforming finite element method for the Biot's consolidation model in poroelasticity*, *J. Comput. Appl. Math.*, 310 (2017), pp. 143–154, <https://doi.org/10.1016/j.cam.2016.06.003>.
- [18] J. J. ILIFF, M. WANG, Y. LIAO, B. A. PLOGG, W. PENG, G. A. GUNDERSEN, H. BENVENISTE, G. E. VATES, R. DEANE, S. A. GOLDMAN, ET AL., *A paravascular pathway facilitates CSF flow through the brain parenchyma and the clearance of interstitial solutes, including amyloid- β* , *Sci. Transl. Med.*, 4 (2012), p. 147ra111.
- [19] N. A. JESSEN, A. S. F. MUNK, I. LUNDGAARD, AND M. NEDERGAARD, *The glymphatic system: a beginner's guide*, *Neurochem. Res.*, 40 (2015), pp. 2583–2599.
- [20] J. KORSÄWE AND G. STARKE, *A least-squares mixed finite element method for Biot's consolidation problem in porous media*, *SIAM J. Numer. Anal.*, 43 (2005), pp. 318–339.
- [21] J. J. LEE, *Robust error analysis of coupled mixed methods for Biot's consolidation model*, *J. Sci. Comput.*, 69 (2016), pp. 610–632, <https://doi.org/10.1007/s10915-016-0210-0>.
- [22] J. J. LEE, *Robust three-field finite element methods for Biot's consolidation model in poroelasticity*, *BIT*, (2017), <https://doi.org/10.1007/s10543-017-0688-3>.
- [23] J. J. LEE, K.-A. MARDAL, AND R. WINTHER, *Parameter-robust discretization and preconditioning of Biot's consolidation model*, *SIAM J. Sci. Comp.*, 39 (2017), pp. A1–A24,

- <https://doi.org/10.1137/15M1029473>.
- [24] C. MICHLER, A. COOKSON, R. CHABINIOK, E. HYDE, J. LEE, M. SINCLAIR, T. SOCHI, A. GOYAL, G. VIGUERAS, D. NORDSLETTEN, ET AL., *A computationally efficient framework for the simulation of cardiac perfusion using a multi-compartment Darcy porous-media flow model*, Int. J. Numer. Method Biomed. Eng., 29 (2013), pp. 217–232.
 - [25] M. A. MURAD, V. THOMÉE, AND A. F. LOULA, *Asymptotic behavior of semidiscrete finite-element approximations of Biot’s consolidation problem*, SIAM J. Numer. Anal., 33 (1996), pp. 1065–1083.
 - [26] T. NAGASHIMA, N. TAMAKI, S. MATSUMOTO, B. HORWITZ, AND Y. SEGUCHI, *Biomechanics of hydrocephalus: a new theoretical model*, Neurosurgery, 21 (1987), pp. 898–904.
 - [27] J. M. NORDBOTTEN, T. RAHMAN, S. I. REPIN, AND J. VALDMAN, *A posteriori error estimates for approximate solutions of the Barenblatt-Biot poroelastic model*, Comput. Methods Appl. Math., 10 (2010), pp. 302–314.
 - [28] R. OYARZÚA AND R. RUIZ-BAIER, *Locking-free finite element methods for poroelasticity*, SIAM J. Numer. Anal., 54 (2016), pp. 2951–2973.
 - [29] P. J. PHILLIPS AND M. F. WHEELER, *A coupling of mixed and continuous Galerkin finite element methods for poroelasticity. I. The continuous in time case*, Comput. Geosci., 11 (2007), pp. 131–144, <https://doi.org/10.1007/s10596-007-9045-y>.
 - [30] E. PIERSANTI AND M. E. ROGNES, *Supplementary material (code) for A mixed finite element method for nearly incompressible multiple- network poroelasticity’ by J. J. Lee, E. Piersanti, K.-A. Mardal and M. E. Rognes.*, Apr. 2018, <https://doi.org/10.5281/zenodo.1215636>.
 - [31] C. RODRIGO, X. HU, P. OHM, J. ADLER, F. J. GASPAR, AND L. ZIKATANOV, *New stabilized discretizations for poroelasticity and the Stokes’ equations*, arXiv preprint arXiv:1706.05169, (2017).
 - [32] R. E. SHOWALTER, *Diffusion in poro-elastic media*, J. Math. Anal. Appl., 251 (2000), pp. 310–340, <https://doi.org/10.1006/jmaa.2000.7048>, <https://doi.org/10.1006/jmaa.2000.7048>.
 - [33] R. E. SHOWALTER AND B. MOMKEN, *Single-phase flow in composite poroelastic media*, Math. Methods Appl. Sci., 25 (2002), pp. 115–139, <https://doi.org/10.1002/mma.276>.
 - [34] C. TAYLOR AND P. HOOD, *A numerical solution of the Navier-Stokes equations using the finite element technique*, Comput. Fluids, 1 (1973), pp. 73–100.
 - [35] B. J. TULLY AND Y. VENTIKOS, *Cerebral water transport using multiple-network poroelastic theory: application to normal pressure hydrocephalus*, J. Fluid Mech., 667 (2011), pp. 188–215.
 - [36] J. C. VARDAKIS, D. CHOU, B. J. TULLY, C. C. HUNG, T. H. LEE, P.-H. TSUI, AND Y. VENTIKOS, *Investigating cerebral oedema using poroelasticity*, Med. Eng. Phys., 38 (2016), pp. 48–57.
 - [37] S.-Y. YI, *Convergence analysis of a new mixed finite element method for Biot’s consolidation model*, Numer. Methods Partial Differential Equations, 30 (2014), pp. 1189–1210, <https://doi.org/10.1002/num.21865>.
 - [38] S.-Y. YI, *A study of two modes of locking in poroelasticity*, SIAM J. Numer. Anal., 55 (2017), pp. 1915–1936.
 - [39] K. YOSIDA, *Functional Analysis*, Springer Classics in Mathematics, Springer-Verlag, 6th ed., 1980.